ANALYSIS AND CALIBRATION OF PARAMETERS OF WET-VISCOUS PADDY MUD PARTICLES BASED ON THE SLUMP EXPERIMENT

/

基于坍落度试验的湿粘性水田泥浆颗粒离散元参数分析及标定

Zhongyi YU [1], Wei XIONG[1], Dequan ZHU[*1,2], Kang XUE[1], Shun ZHANG[1], Fuming KUANG[1], Jinnan QUE[1], Xiaoshuang ZHANG[1], Ben HENG[1]

[1] College of Engineering, Anhui Agricultural University, Hefei 230036, China;

[2] Anhui Province Engineering Laboratory of Intelligent Agricultural Machinery and Equipment, Hefei 230036, China;

[*] *Corresponding author: Dequan Zhu, E-mail: zhudequan@ahau.edu.cn*

DOI: https://doi.org/10.35633/inmateh-68-18

***Keywords**: Slump test, Mud particles, Response surface methodology, DEM, Parameter calibration*

ABSTRACT

In order to obtain the discrete element contact parameters of wet and viscous paddy field mud particles, an accurate numerical simulation model was constructed. In order to obtain the discrete element contact parameters of wet and viscous paddy field mud particles, an accurate numerical simulation model was constructed.Firstly, the paddy field mud with an average particle size of 0.2 mm was taken as the research object, and the basic physical parameters and rheological behavior laws were obtained through physical measurements and rotational rheological tests. Based on the slump test, combined with the particle scaling theory and Johnson-Kendall-Roberts (JKR) model, and the slump and slump-flow values were taken as response values, the Plackett-Burman test, the steepest climb test and the Box-Behnken test were designed by Design-Expert software to complete the simulation parameters calibration. The optimal significance parameters are as follows: 0.096 J/m^2 for the JKR surface energy of mud, 0.13 for the mud-mud restitution coefficient and 0.6 for the mud-steel static friction coefficient. Finally, the mud slump and fluidity verification tests showed that the relative errors between the simulation values and the physical values of slump and slump-flow are 1.73% and 0.42%, and the average error of torque is 2.47%, and the parameters are accurate and reliable. The calibration method can accurately construct the discrete element model of wet-viscous particles, which provides basic data and technical guidance for the coupling mechanism of paddy machinery-mud.

摘要

为获取湿黏性的水田泥浆颗粒离散元接触参数，构建精准的数值仿真模型。首先，以平均粒径为 0.2 mm 水田泥浆为研究对象，通过物理测定和旋转流变试验，得出基本物理参数和流变行为规律。基于坍塌物理试验，结合颗粒缩放理论和 JKR 接触模型，以塌落度和拓展度为响应值，采用 Design Expert 软件依次设计 Plackett-Burman 试验、最陡爬坡试验和 Box-Behnken 试验，进行仿真参数标定。显著性参数最优值为泥浆 JKR 表面能为 0.096 J/㎡、泥浆-泥浆恢复系数为 0.13 和泥浆-钢静摩擦系数 0.6。最后，水田泥浆塌落和流变验证试验表明，塌落度和拓展度仿真与物理值的相对误差为 1.73%、0.42%，扭矩平均误差为 2.47%，标定参数准确可靠。本文提出的标定方法能够精确地构建湿黏性颗粒-泥浆离散元模型，为机械-泥浆耦合机理提供基础数据和技术指导。

INTRODUCTION

At present, the bed soil with high water content and no surface water is used in rice seedlings in order to cultivate stronger machine-planted rice seedlings, which is in line with the characteristics of rice planting mechanization in southern China (*Li et al., 2018; Ye., 2021*). Compared with ordinary soil, paddy mud is sticky and heavy, with stronger swelling and flow plasticity, leading to adhesion problems of soil-touching parts in the field and seriously affects production efficiency. Due to the complexity of paddy mud structure and the importance of developing soil-touching parts, it is necessary to analyze the interaction coupling mechanism between them. However, the macroscopic physical test cannot prove the microscopic motion law of mud

[1] *Zhongyi Yu, As. M.S. Stud. Eng.; Wei Xiong, Ph.D. Eng.; Dequan Zhu, Prof. Ph.D. Eng.; Kang Xue, As. Ph.D. Stud. Eng.; Shun Zhang, Prof. Ph.D. Eng.; Fuming Kuang, Prof. Ph.D. Eng.; Jinnan Que, As. M.S. Stud. Eng.; Xiaoshuang Zhang, As. M.S. Stud. Eng.;*

particles, and the research is generally carried out using numerical simulation.

Since the finite element method simulates the overall disruptive behavior of the mud in the form of a continuous medium, it is impossible to analyze the movement process of mud particles. The research shows that the discrete element method based on the principle of particle contact mechanics is suitable for soil particle groups with power-law rheological characteristics, especially wet soil or paddy mud with complex composition and rheological properties (*Xu et al., 2003; Tamás K et al., 2013*).

Generally, simulation parameters need to be determined before constructing the discrete element numerical model. The material intrinsic parameters are obtained from references, material contact, and model parameters are obtained by direct measurements or calibration of virtual tests. Due to the limitations of test conditions and methods, it is difficult to obtain accurate contact parameters through actual tests. Most research concentrated on using virtual simulation experiments to obtain the contact parameters of wet and viscous materials, and a large number of virtual calibration simulation experiments have been performed (*Du et al., 2021; Zhang et al., 2022; Wang et al., 2021; Zheng et al., 2021*). An optimization method based on a regression model was established by combining physical experiments, to address the difficult problem of obtaining the contact characteristic parameters used in the DEM model of quinoa grains and for calibrating the parameters of the quinoa DEM model *(Liu et al., 2020).* An accurate clay loam discrete element simulation model was constructed based on the accumulation test, which provided technical support for the research on the dynamics of soil-contacting parts (*Xiang et al., 2019)*. Based on the DEM numerical model, a method for simulations of soil flow properties was proposed using the discrete element method (DEM) (*Qi L. et al., 2019)*. The simulation optimization design experiments and physical experiments were combined to calibrate the parameters of simulated discrete element of buckwheat seeds *(Xu B.et al., 2021)*. The Hertz-Mindlin with bonding contact model was used to calibrate the parameters of soils in Inner Mongolia, and to solve dynamic soil behavior at the contact interface, which makes it difficult to ensure transplanting quality during transplanting (*Zeng et al., 2021)*. Based on the theory of particle scaling, the contact parameters of seeds, powders, and between powders and seeds were calibrated to provide a reference to the discrete element simulation parameter calibration of similar fine particles and powders materials (*Ma et al., 2022)*. The Johnson-Kendall-Roberts (JKR) contact model was applied to construct and calibrate the parameters of wet sand and gravel particles in the screening process, which provided theoretical guidance for studying the modeling of wet particles and improving the screening efficiency (*Zhou JC et al., 2022)*. Although wet material particles have been widely studied by different methods and means, there is still little research on discrete element simulation modeling and parameter calibration of paddy mud with complex components, high water content, and micro-sized particle, and the aforementioned methods are not applicable.

Therefore, the approaches to accurately obtain the contact parameters between the mud particles and that between the mud particles and the working parts on the transplanter were studied. The contact and model parameters of paddy mud simulation were calibrated, combined with the advantages of discrete element technology in the nonlinear simulation of wet granular materials. The findings can be applied to the numerical simulation research of paddy field machinery. Given the large number and small particle size of paddy mud in southern China, particle scaling theory engineering technology is used to enlarge the particles in the original system to reduce the number of discrete units in the model and to carry out effective simulation and calculation (*Li et al., 2019*). In addition, paddy mud is difficult to accumulate due to its good fluidity, the slump test can be used to measure the fluidity and consistency by observing the slumped shape of the mud under the action of self-weight *(Wang et al., 2022; Coetzee, 2017)*. A method combining discrete element virtual simulation and slump physical test was proposed to calibrate wet-viscous mud particles' contact and model parameters based on the particle scaling theory and the JKR contact model. The accuracy of simulation parameters was verified by field test and the fluidity test, in order to build an accurate discrete element numerical model of wet-viscous mud in southern China.

MATERIALS AND METHODS

Basic physical parameters of test materials

The paddy mud samples were collected from Feixi County, Anhui Province, China. The particle volume fraction distribution of mud was determined by Mastersizer 2000 particle analyzer (*Wang et al., 2014*), as shown in Fig.1. The average particle size was calculated to be 0.2 mm. The basic physical parameters of paddy mud were determined through a drying test and mud hydrometer and liquid plastic limit measurement test, which were shown in Table 1.

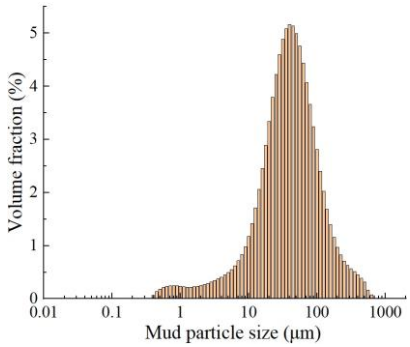

Fig. 1 - Particle size distribution of paddy mud

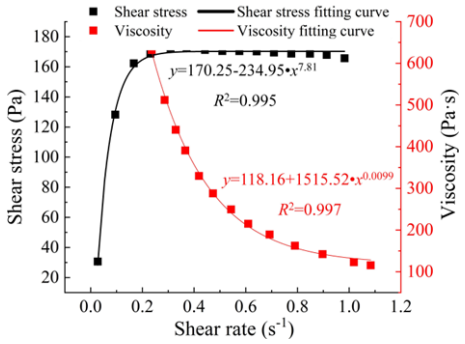

Fig. 2 - Fitting curves of mud at 38% water content

Table 1

Basic parameters of physical mud

Particle size distribution /%			Liquid limit (%)	Plastic limit (%)	Plasticity index (%)	Proportion (g·cm^{-3})	Moisture content (%)
cohesive grain (0-2 μm)	powder grain (2-20 μm)	sand grain (20-2000 μm)					
38.24	19.61	42.61	15.67	26.10	10.43	1.68	38

Experimental study on rheological properties of paddy mud

Rheological tests can describe the rheological behavior of wet and viscous materials (e.g., concrete and mud) and clarify the functional relationship between the characteristic parameters of shear stress or viscosity *(Yang et al., 2017)*. The shear rate-stress and shear rate-viscosity function curves of mud samples with a water content of 38% were obtained via the Brookfield R/S plus rheometer, in order to study the rheological behavior characteristics and parameter change low of paddy mud, as shown in Fig. 2.

In Fig. 2, the shear stress of the sample shows a tendency of increasing with the shear rate, which is consistent with the basic law of rheology. After reaching a certain level, the mud shows a strong shear dilution, leading to a slow decrease in shear stress. As the shear rate increases, the gap between particles increases during the flow of mud, resulting in the decrease of adhesion and the gradual decrease of viscosity. Therefore, the sample mud is a non-Newtonian fluid with power-law rheological characteristics, which is suitable for numerical simulation of the discrete element method *(Sun, 2017)*. The Herschel-Bulkley constitutive equation of the mud sample was fitted, as illustrated in Eq. (1), where τ is the shear stress, τ_0 is the yield stress, K is the viscosity coefficient, D is the shear rate, and n is the flow indicator.

$$\tau = \tau_0 + K \cdot (D)^n \tag{1}$$

Physical test of paddy mud slump

Abrams has proposed that the slump test can characterize the rheological parameters of fluidity and viscosity through the slump and slump-flow of materials *(Sun, 2017)*. The slump test of paddy mud refers to the "Standard for Test Methods for the Performance of Ordinary Concrete Mixtures" *(GB/T 50080-2016, 2016)*, and the test tools and process are shown in Fig. 3.

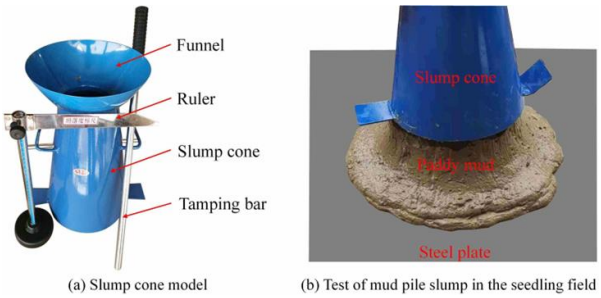

Fig. 3 - Physical test of mud pile slump

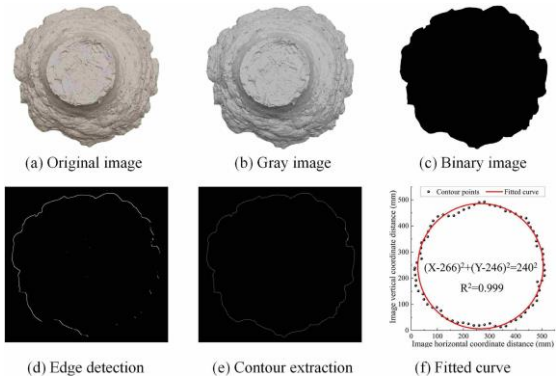

Fig. 4 - Image processing of slump-flow

The average value of 10 test values of 231 mm mud was taken as the measured slump value to reduce the ruler measurement errors.

The grayscale processing, binarization processing, edge detection, and contour extraction sequence were performed on the obtained original image of slump-flow, in order to more accurately measure the slump-flow values of mud piles with uneven surfaces and boundaries. Edge contour pixel points were converted into real coordinate data, and the equation of the circle curve function was fitted. The approximate circle diameter of 480 mm was taken as the slump-flow value, as shown in Fig. 4.

Slump test simulation model modeling

The virtual slump test of paddy mud was performed in EDEM 2018 software, and the model parameters were continuously adjusted until the mechanical behavior and flow states of the model were consistent with reality. It can be considered that the parameters of the discrete element model are consistent with the actual situation *(Zeng et al., 2021)*. The slump and slump-flow values were measured when the velocity of mud particles was approximately zero and no significant flow occurred, as shown in Fig. 5(a). The Hertz-Mindlin (no slip) contact model was chosen as the contact model between mud particles and steel. The mud and steel intrinsic parameters are listed in Table 2 *(Ghosh et al., 2021; Hao et al., 2020)*.

Since the size of paddy mud is micron level, increasing the particle radius or calculation time step is beneficial to improve the simulation efficiency *(Zhang et al., 2022)*.

The calculation formula of Rayleigh time step T_R is shown in Eq. (2).

$$T_R = \frac{\pi R}{(0.163\nu + 0.877)}\sqrt{\left(\frac{\rho}{G}\right)} \tag{2}$$

where R is the particle radius, ρ is the mud density, G is the shear modulus, and ν is the Poisson's ratio of mud.

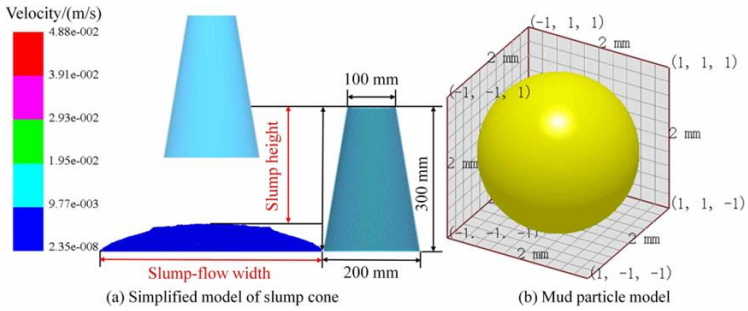

Fig. 5 - EDEM virtual slump test model

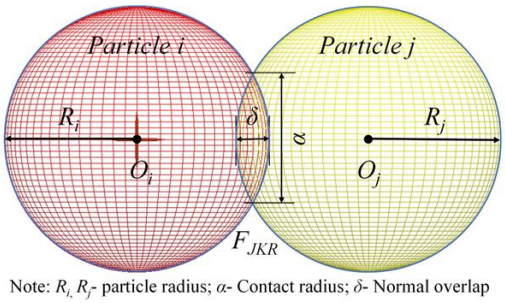

Fig. 6 - Diagram of particles in JKR contact

Table 2

Intrinsic parameters of mud particles and steel

Materials	Poisson's ratio	Density (kg·m^{-3})	Shear modulus (MPa)
Mud	0.5	1680	1
Steel	0.3	7800	7000

Mud particles contact model selection

The paddy mud studied in this paper has a high water content due to long-term soaking, and the adhesion between particles leads to complex and diverse mechanical behaviors of paddy mud. The Hertz-Mindlin with JKR cohesion contact model can better characterize the obvious adhesion and agglomeration between particles due to electrostatic force and water content, which is suitable for moisture-containing materials with significant bonding and agglomeration caused by moisture (*Li et al., 2019; Rojek et al., 2019*), as shown in Fig. 6.

The normal cohesive force of the model, F_{JKR}, relates to the amount of normal overlap δ, interaction parameters, and cumulative surface energy density γ (J/m^2).

The expressions are as follows:

$$F_{JKR} = -4\sqrt{\pi\gamma E^*}\alpha^{\frac{3}{2}} + \frac{4E^*}{3R^*}\alpha^3 \tag{3}$$

$$\delta = \frac{\alpha^2}{R^*} - \sqrt{\frac{4\pi\gamma\alpha}{E^*}} \tag{4}$$

$$\frac{1}{E^*} = \frac{\left(1-\nu_i^2\right)}{E_i} + \frac{\left(1-\nu_j^2\right)}{E_j} \tag{5}$$

$$\frac{1}{R^*} = \frac{1}{R_i} + \frac{1}{R_j} \tag{6}$$

where α is the tangential overlap between the two particles, E^* and R^* are the equivalent radius and equivalent Young's modulus, E_i, ν_i, and R_i are the elastic modulus, Poisson's ratio, and radius of particle i; E_j, ν_j, and R_j are the elastic modulus of particle j.

The separation force $F_{abruption}$ required to separate the two particles depends on the surface tension γ_s and wetting angle θ.

$$F_{abruption} = -2\pi\gamma_s \cos(\theta)\sqrt{R_i R_j} \tag{7}$$

The paddy mud particles were set to spherical particles with a diameter of 2 mm by using the particle contact scaling principle on the calculation capability and simulation model reliability of the software (*Li et al., 2019; Coetzee., 2017; Zhang et al., 2022; Roessler et al., 2018*). A simplified slump cone simulation model was built with the actual size, as shown in Fig. 5. After several simulation pre-tests and physical tests, it was determined that the ascending speed of the slump cone was 0.05 m/s, 0.9 million particles were generated, and the total simulation time was 5 s. The test process is shown in Fig. 7.

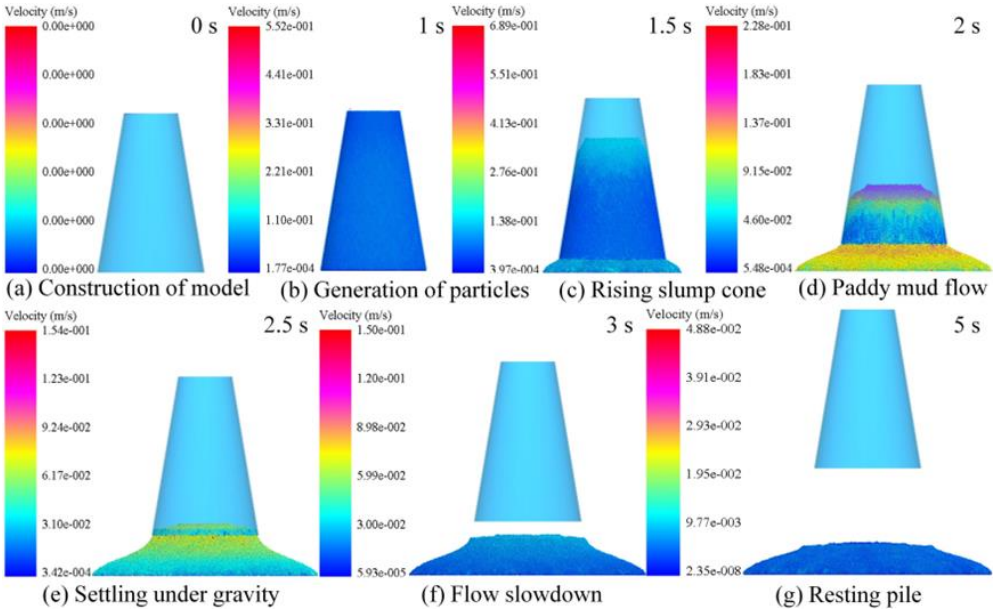

Fig. 7 - The simulation test process of paddy mud's slump and slump-flow

RSM test for simulation parameters calibration

The Plackett-Burman test was performed to identify the parameters with significant influence. Combined with a large number of pre-tests, the eigen parameters of paddy mud were entered into the EDEM 2018 Generic material model database (GEMM), and the range of contact parameters was determined, as shown in Table 3. There were 7 real parameters (H_1 to H_7) and 4 virtual parameters (H_8 to H_{11}) in the simulation test. Each parameter was set to a low and high level, which were represented by codes -1 and +1, respectively.

According to the significant parameters obtained from the Plackett-Burman test, the steepest climb test was designed to reduce the number of tests and find the level ranges of the best response values. The relative errors δ_t between the simulation value and the physical value of the slump or slump-flow were taken as the evaluation indicators, respectively. The calculation formula for the relative errors δ_t is as follows:

$$\delta_t = \frac{\left|Y_t - Y_t'\right|}{Y_t'} \tag{8}$$

where Y_t is the measured value of slump Y_1 or slump-flow Y_2, and Y_t' is the simulation value of slump Y_1' or slump-flow Y_2'.

Table 3

The parameter table of the Plackett-Burman test

Symbol	Simulation parameters	Parameter levels		
		-1	0	1
H_1	Mud-mud restitution coefficient	0.01	0.055	0.1
H_2	Mud-mud static friction coefficient	0.1	0.15	0.2
H_3	Mud-mud rolling friction coefficient	0.05	0.125	0.2
H_4	Mud-steel restitution coefficient	0.1	0.3	0.5
H_5	Mud-steel static friction coefficient	0.2	0.35	0.5
H_6	Mud-steel rolling friction coefficient	0.01	0.055	0.1
H_7	JKR surface energy of mud ($J \cdot m^{-2}$)	0.02	0.06	0.1
H_8, H_9, H_{10}, H_{11}	Virtual parameters	-1	0	1

Box-Behnken test was used to express the second-order regression equation between the significance parameters and response values by response surface methodology (RSM). The high, medium, and low levels of significance parameters were set to +1, 0, and -1. The non-significant parameters take the middle value of each factor in Table 3. The 5 center points were used to estimate the error, and the 17 tests were performed in total. Each set of simulation tests was repeated 3 times, and the average value was recorded as the numerical result of the simulation tests.

RESULTS AND DISCUSSION

Plackett-Burman test

Taking the slump and slump-flow values of paddy mud as the response values, the Plackett Burman test was designed by Design-Expert 12 software. The 13 groups of tests are performed, as shown in Table 4.

Table 4

Scheme and results of Plackett-Burman test

No.	Test factors											Slump Y_1 (mm)	Slump-flow Y_2 (mm)
	H_1	H_2	H_3	H_4	H_5	H_6	H_7	H_8	H_9	H_{10}	H_{11}		
1	-1	-1	-1	-1	-1	-1	-1	-1	-1	-1	-1	265	635
2	1	1	1	-1	-1	-1	1	-1	1	1	-1	249	596
3	-1	1	-1	1	1	-1	1	1	1	-1	-1	252	518
4	-1	1	1	-1	1	1	1	-1	-1	-1	1	247	478
5	-1	1	1	1	-1	-1	-1	1	-1	1	1	262	622
6	1	-1	1	1	-1	1	1	1	-1	-1	-1	248	592
7	1	-1	1	1	1	-1	-1	-1	1	-1	1	244	495
8	-1	-1	1	-1	1	1	-1	1	1	1	-1	253	496
9	-1	-1	-1	1	-1	1	1	-1	1	1	1	258	608
10	1	1	-1	-1	-1	1	-1	1	1	-1	1	255	606
11	1	1	-1	1	1	1	-1	-1	-1	1	-1	246	496
12	1	-1	-1	-1	1	-1	1	1	-1	1	1	237	480
13	0	0	0	0	0	0	0	0	0	0	0	245	505

The significant result of each parameter was obtained, as shown in Table 5 and Fig. 8. It can be seen that the restitution coefficient (H_1) of mud-mud, the static friction coefficient (H_5) of mud-steel, and the JKR surface energy of mud (H_7) have significant effects on the simulated slump and slump-flow, while other simulation parameters have no significant effect on them.

Table 5

Significance analysis of Plackett-Burman test results

Indexes	Sources of variation	Sum of squares	Degrees of freedom	Mean square	*F*-value	*P*-value	Significance ranking
Slump (mm)	Model	670	7	95.71	26.1	0.0035**	
	H_1	280.33	1	280.33	76.45	0.0009**	1
	H_2	3	1	3	0.82	0.4169	5
	H_3	8.33	1	8.33	2.27	0.2062	4
	H_4	1.33	1	1.33	0.36	0.579	6
	H_5	280.33	1	280.33	76.45	0.0009**	1
	H_6	0.33	1	0.33	0.09	0.778	7
	H_7	96.33	1	96.33	26.27	0.0069**	3
	Curvature	37.03	1	37.03	10.1	0.0336*	
	Residual	14.67	4	3.67			
	Total sum	721.69	12				
	R_1^2=0.9786; $R_1^2{}_{adj}$=0.9411; CV=0.76%; Adeq Precision=15.6911						
Slump-flow (mm)	Model	42471.67	7	6067.38	100.29	0.0003**	
	H_1	705.33	1	705.33	11.66	0.0269*	2
	H_2	8.33	1	8.33	0.14	0.7294	7
	H_3	341.33	1	341.33	5.64	0.0764	5
	H_4	133.33	1	133.33	2.20	0.2118	6
	H_5	40368.00	1	40368.00	667.24	<0.0001	1
	H_6	408.33	1	408.33	6.75	0.0603	4
	H_7	507.00	1	507.00	8.38	0.0443*	3
	Curvature	2024.64	1	2024.64	33.47	0.0044**	
	Residual	242.00	4	60.50			
	Total sum	44738.31	12				
	R_2^2=0.9943; $R_2^2{}_{adj}$=0.9844; CV=1.42%; Adeq Precision=23.1259						

*Note: **means the item is extremely significant ($P < 0.01$), *means the item is significant ($0.01 \leq P < 0.05$), and $P \geq 0.05$ means the item is insignificant.*

The steepest climb test

Considering the range of three significant parameters, i.e., H_1 (A), H_5 (B), and H_7 (C) obtained from the Plackett-Burman test ($P < 0.05$), each step length of the steepest climb test was set as follows: ΔA was 0.03, ΔB was 0.1, and ΔC was 0.03. The results are shown in Table 6.

With the gradual increase of the significance parameter, the slump and slump-flow gradually decrease, and the relative errors between the real test and the simulation gradually decrease. The relative error of the 4th test was the smallest and less than 5%, which meets the experimental requirements. Therefore, the parameter of the 4th test was chosen to be the intermediate level (0), and the parameter of the 3rd test was chosen as the low level (-1). A set of parameters with equal step length was selected as the high level (+1) for the subsequent response surface design. The low, medium and high levels of parameters A, B and C are 0.07, 0.1, and 0.13; 0.4, 0.5, and 0.6; 0.07 J/m^2, 0.1 J/m^2 and 0.13 J/m^2, respectively.

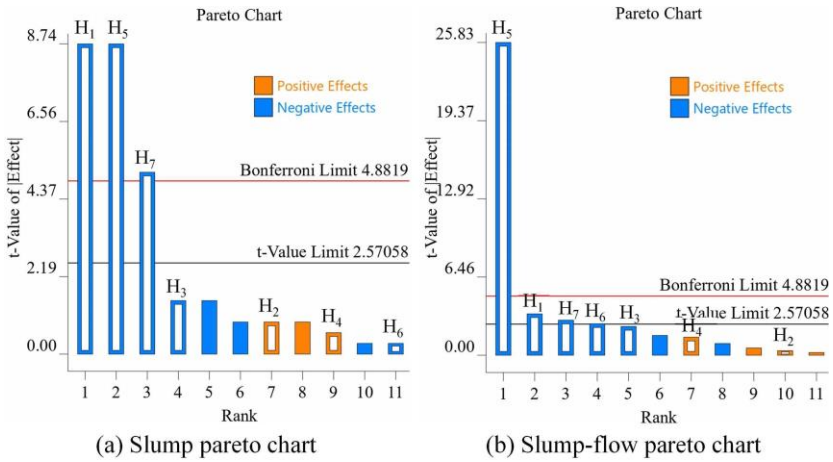

(a) Slump pareto chart (b) Slump-flow pareto chart

Fig. 8 - Slump and slump-flow Pareto chart

Table 6

Scheme and results of steepest climb test

No.	Test factors			Slump Y_1 (mm)	Relative errors δ_1 (%)	Slump-flow Y_2 (mm)	Relative errors δ_2 (%)
	A	*B*	*C*				
1	0.01	0.2	0.01	258	11.69	612	27.50
2	0.04	0.3	0.04	249	7.79	537	11.88
3	0.07	0.4	0.07	245	6.06	503	4.79
4	0.10	0.5	0.10	242	4.76	485	1.04

Note: Parameters A, B, and C are equal to test factors H_1、H_5、H_7, respectively.

Box-Behnken test

Table 7

Design and results of Box-Behnken test

No.	Factors			Slump Y_1 (mm)	Relative errors δ_1 (%)	Slump-flow Y_2 (mm)	Relative errors δ_2 (%)
	A	*B*	*C*				
1	1(0.13)	1	0	236	2.16	474	1.25
2	1	-1	0(0.1)	240	3.90	494	2.92
3	1	0(0.5)	-1	249	7.80	534	11.25
4	1	0	1	236	2.16	468	2.50
5	-1(0.07)	-1	0	242	4.76	498	3.75
6	-1	1(0.6)	0	244	5.63	490	2.08
7	-1	0	-1(0.07)	243	5.19	488	1.67
8	-1	0	1	250	8.23	524	9.17
9	0(0.1)	1	1	237	2.60	470	2.08
10	0	1	-1	243	5.19	492	2.50
11	0	-1	1(0.13)	243	5.19	496	3.33
12	0	-1(0.4)	-1	241	4.33	498	3.75
13	0	0	0	244	5.63	484	0.83
14	0	0	0	243	5.19	486	1.25
15	0	0	0	244	5.63	488	1.67
16	0	0	0	244	5.63	484	0.83
17	0	0	0	244	5.63	486	1.25

Note: Numbers in brackets are the values of test factor levels.

The Box-Behnken test was applied to conduct response surface analysis and find the optimal solution. The values of other non-significant parameters were the same as those in the steepest climbing test. The test protocol and results are shown in Table 7.

Response surface regression modeling and ANOVA

Multiple regression fitting analysis of the slump test results was performed via Design-expert 12 software, as shown in Table 8.

Table 8

ANOVA of the quadratic polynomial model of the Box-Behnken test

Indexes	Source of Variance	Sum of Squares	Degree of freedom	Mean Square	*F*-value	*P*-value
Slump Y_1 (mm)	Model	231.94	9	25.77	78.43	<0.0001**
	A	40.5	1	40.5	123.26	<0.0001**
	B	4.5	1	4.5	13.7	0.0076**
	C	12.5	1	12.5	38.04	0.0005**
	AB	9	1	9	27.39	0.0012**
	AC	100	1	100	304.35	<0.0001**
	BC	16	1	16	48.7	0.0002**
	A^2	0.04	1	0.04	0.13	0.7309
	B^2	48.67	1	48.67	148.14	<0.0001**
	C^2	1.52	1	1.52	4.61	0.0688
	Residual	2.3	7	0.33		
	Lack of fit	1.5	3	0.5	2.5	0.1985
	Pure error	0.8	4	0.2		
	Sum	234.24	16			
	R_1^2=0.9902; $R_1^2{}_{adj}$=0.9776; CV=0.2363%; Adeq Precision=32.9820					
Slump-flow Y_2 (mm)	Model	4463.92	9	495.99	114.96	<0.0001**
	A	112.5	1	112.5	26.08	0.0014**
	B	450	1	450	104.3	<0.0001**
	C	364.5	1	364.5	84.49	<0.0001**
	AB	36	1	36	8.34	0.0234*
	AC	2601	1	2601	602.88	<0.0001**
	BC	100	1	100	23.18	0.0019**
	A^2	337.27	1	337.27	78.18	<0.0001**
	B^2	129.69	1	129.69	30.06	0.0009**
	C^2	337.27	1	337.27	78.18	<0.0001**
	Residual	30.2	7	4.31		
	Lack of fit	19	3	6.33	2.26	0.2234
	Pure error	11.2	4	2.8		
	Sum	4494.12	16			
	R_2^2=0.9933; $R_2^2{}_{adj}$=0.9846; CV=0.4227%; Adeq Precision=40.4883					

*Note: ** and * indicated significance at 0.01 and 0.05 levels, respectively.*

A second-order regression model of the simulated slump Y_1 and slump-flow Y_2 of paddy mud was built, and the significant parameters were obtained. The regression model is expressed as follows:

$$\begin{cases} Y_1 = 243.8 - 2.25A - 0.75B - 1.25C - 1.5AB - 5AC - 2BC + 0.1A^2 - 3.4B^2 + 0.6C^2 \\ Y_2 = 485.6 - 3.75A - 7.5B - 6.75C - 3AB - 25.5AC - 5BC + 8.95A^2 - 5.55B^2 + 8.95C^2 \end{cases} \quad (9)$$

Table 8 shows the model with $P < 0.0001$, indicating the regression models of slump and slump-flow are extremely significant. It can be seen that the quadratic term (B^2), the restitution coefficient (A) of mud-mud, the static friction coefficient (B) of mud-steel, the JKR surface energy of mud (C), and their interaction terms have extremely significant effects on the slump and the slump-flow. The quadratic terms A^2 and C^2 have no significant effect on the slump ($P > 0.05$). The lack-of-fit term $P > 0.05$, the variation coefficient of 0.2363% and 0.4227% are low, indicating the two equations fit well. The coefficients of determination, R_1^2, equals 0.9902, and R_2^2, equals 0.9933; the correction coefficients of determination, $R_1^2{}_{adj}$, equals 0.9776, and $R_2^2{}_{adj}$, equals 0.9846. All of the coefficients are close to 1, indicating the fitting equations are highly reliable. The precisions are 32.982 and 40.4883, respectively, indicating the accuracy of the model is good.

Interaction effect analysis

To explore the interaction effect of three significant parameters on the predicted response values, the interaction term response surface and contour distribution map of the slump and slump-flow were obtained. As shown in Fig. 9, the curvature of the response surface shows that the order of influence of the interaction term is $AC > BC > AB$, where AC refers to the interaction between A and C, and so on.

(1) Analysis of interaction effect on the slump

From Fig. 9(a), the slump decreases with the increase of the mud-mud restitution coefficient, and increases first and then decreases abruptly with the increase of the mud-steel static friction coefficient. However, the response surface varies faster along the direction of the mud-mud restitution coefficient than the direction of the mud-steel static friction coefficient. From Fig. 9(b), the slump decreases sharply with the increase of the mud-mud restitution coefficient and the JKR surface energy of mud, and the effect is significant. From Fig. 9(c), the slump first increases and then decreases sharply with the increase of the mud-steel static friction coefficient, and decreases with the increase of the JKR surface energy of mud.

(2) Analysis of interaction effect on slump-flow

From Fig. 9(d), the slump-flow increases with the increase of the mud-mud restitution coefficient, and decreases with the increase of the mud-steel static friction coefficient. From Fig. 9(e), the mud-mud restitution coefficient and the JKR surface energy of mud increase, the slump-flow rapidly decreases, and the impact is significant. From Fig. 9(f), the slump-flow decreases with the increase of the mud-steel static friction coefficient, and first decreases and then increases with the increase of the JKR surface energy of mud.

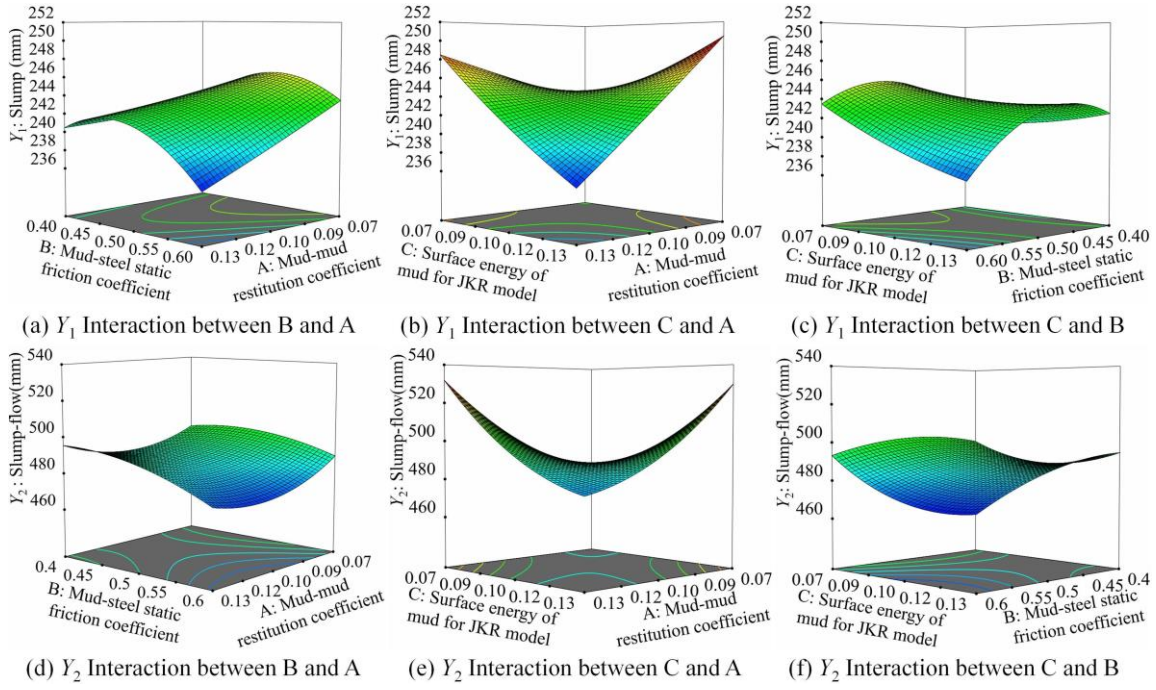

(a) Y_1 Interaction between B and A (b) Y_1 Interaction between C and A (c) Y_1 Interaction between C and B

(d) Y_2 Interaction between B and A (e) Y_2 Interaction between C and A (f) Y_2 Interaction between C and B

Fig. 9 - Effects of interactive factors on slump and slump-flow

Overall, the response surface curve of the mud-mud restitution coefficient (*A*) and the JKR surface energy of mud (*C*) are steepest, indicating they have a more significant impact on the slump and the slump-flow. The result is consistent with that of variance analysis of the regression model.

Determining the optimal parameters

The regression model and simulation parameters were optimized; the measured slump of 231 mm mud and the slump-flow of 480 mm mud were used as the target values for the verification of simulation tests. The corresponding objective and constraint equations are as follows:

$$Obj.\begin{cases} Y_1(A,B,C)=231 \\ Y_2(A,B,C)=480 \end{cases}$$
$$s.t.\begin{cases} 0.07 \le A \le 0.13 \\ 0.4 \le B \le 0.6 \\ 0.07 \le C \le 0.13 \end{cases} \quad (10)$$

A set of optimal solutions that are similar to the actual physical slump and slump-flow data were obtained, and the result data were 0.13 for the mud-mud restitution coefficient, 0.6 for the mud-steel static friction coefficient, 0.096 J/m^2 for the JKR surface energy of mud, and values of the rest non-significant parameters are the same as those in the steepest climbing test. The optimal values of each parameter and response indexes are shown in Fig. 10.

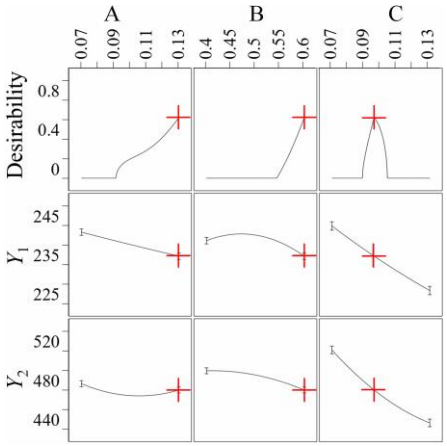

Fig. 10 - Ramp function graph for parameters and response value

Validation test

From Fig. 11, the predicted values of the slump and the slump-flow under the optimal solution of regression fitting are 237 mm and 480 mm, respectively. The mean relative errors are 0.85% and 0.42% with the simulation test results, respectively.

Fig. 12 describes the comparison between the simulated and measured values of the slump and the slump-flow under the optimal parameters. The average relative errors with the simulation test are only 1.73% and 0.42%.

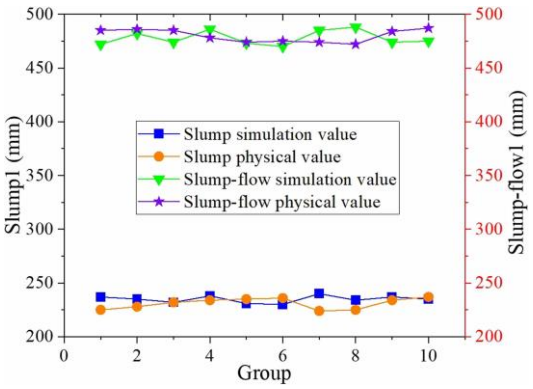

Fig. 11 - Comparison between physical and simulation results of paddy mud slump and slump-flow

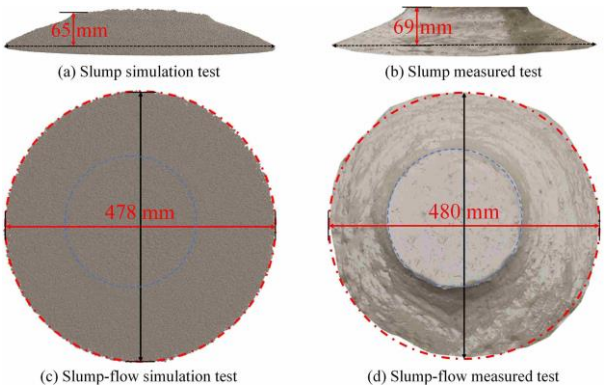

Fig. 12 - Comparison of physical test and simulation test

To further identify the accuracy and rationality of calibrated model parameters, the aforementioned R/S plus rheometer was used to perform the paddy mud fluidity verification test. The target of the test was the rotor blade torque, and the rheological properties of mud were selected as the verification indicator *(Han et al., 2021)*. A simplified model of the rheological test was constructed in EDEM software *(Nan et al., 2020)*. The simulation test was performed on the calibrated optimal parameters, and blade torque data after smooth rotation of mud was derived. The experimental device and simulation test model are shown in Fig. 13.

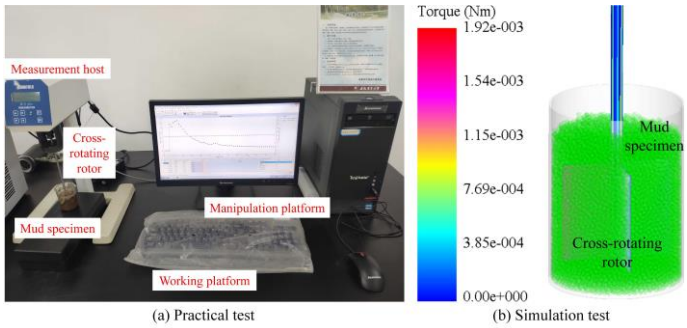

Fig. 13 - The validation test process of paddy mud fluidity

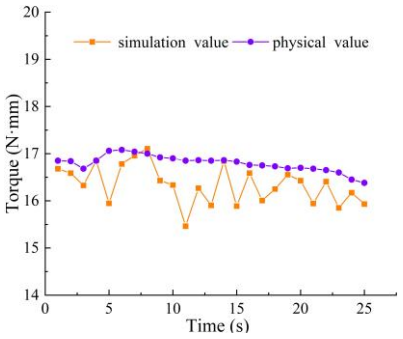

Fig. 14 - Simulation and physical results of paddy mud flow torque

Fig. 14 shows a comparative analysis of the blade torque in mud flow in the measured and simulated values with an average relative error of 2.47%, indicating that the bulk rheological properties of paddy mud in the simulation model are consistent with the actual, and the built discrete element model of wet particles is reliable.

CONCLUSIONS

(1) Taking the paddy field mud in southern China as an example, a method for systematically obtaining the calibration and optimization of discrete element simulation parameters of wet-viscous mud particles is proposed, which is based on the combination of slump physical test and DEM virtual simulation. The method can construct an accurate discrete element simulation model of paddy mud in southern China.

(2) Taking the slump and the slump-flow as the response values, the simulation parameters were calibrated and optimized by significance analysis and response surface method. The optimal parameters were obtained, and the result data were 0.13 for the mud-mud restitution coefficient, 0.6 for the mud-steel static friction coefficient, and 0.096 J/m2 for the JKR surface energy of mud. The remaining non-significant parameters include the mud-mud static friction coefficient is 0.15, the mud-mud rolling friction coefficient is 0.125, the mud-steel restitution coefficient is 0.3 and the mud-steel rolling friction coefficient is 0.055. Finally, the accuracy of the constructed discrete element simulation model of mud particles was verified by the physical slump test and fluidity test. The results of the research can provide basic data and technical support to investigate the rheological behavior and dynamic characteristics of the mud-mechanical components of the paddy field.

(3) The verification tests of paddy mud slump and fluidity show that paddy mud is a non-Newtonian fluid with power-law rheological characteristics. The relative errors between the simulation and physical values of slump and slump-flow are 1.73% and 0.42% respectively. The average relative error of rotational torque is 2.47%, which indicate that the method of parameter calibration and research results are accurate and reliable.

ACKNOWLEDGEMENTS

This work was supported by the Natural Science Foundation of Anhui Province (Grant No. 2208085ME131), Major Science and Technology Project of Anhui Province (Grant No. 202203a06020004), Postgraduate Scientific Research Projects of Universities in Anhui Province (Grant No. YJS20210233), Innovation and Entrepreneurship Training Program for College Students of Anhui Agricultural University (Grant No. X202210364564) and Key common technology research and development projects in Hefei (Grant No. 2021GJ078).

REFERENCES

[1] Coetzee C.J., (2017). Review: Calibration of the Discrete Element Method. *Powder Technology*, No. 310, pp. 104-142.

[2] Du X., Liu C.L., Jiang M. et al., (2021). Calibration of bonding model parameters for coated fertilizers based on PSO-BP neural network. *INMATEH-Agricultural Engineering*, Vol.65, No. 3, pp.255-264.
[3] GB/T 50080-2016., (2016). Standard for test method of performance on ordinary fresh concrete. Ministry of Housing and Urban-Rural Development of the Peoples Republic of China.
[4] Ghosh P., Anan G. K., (2021). Discrete element modeling of cantilever beams subjected to geometric nonlinearity and particle–structure interaction. *Computational Particle Mechanics*, No. 8, pp. 1-15.
[5] Han J.G., Bi Y., Yan P.Y. et al., (2021). Acquisition of Bingham fluid rheology parameters using a coaxial double-cylinder rheometer. *Journal of the Chinese Ceramic Society*, Vol.49, No. 2, pp. 323-331.
[6] Hao J.J., Long S.F., Li J.C. et al., (2020). Effect of granular ruler in discrete element model of sandy loam fluidity in Ma yam planting field. *Transactions of the Chinese Society of Agricultural Engineering*, Vol.36, No. 21, pp. 56-64.
[7] Li J.W., Tong J., Hu B. et al., (2019). Calibration of parameters of interaction between clayey black soil with different moisture content and soil-engaging component in northeast China. *Transactions of the Chinese Society of Agricultural Engineering*, Vol.35, No. 6, pp. 130-140.
[8] Li Y.X., Li F.X., Xu X.M. et al., (2019). Parameter calibration of wheat flour for discrete element method simulation based on particle scaling. *Transactions of the Chinese Society of Agricultural Engineering*, Vol.35, No. 16, pp. 320-327.
[9] Li Z.H., Ma X., Li X.H. et al., (2018). Research Progress of Rice Transplanting Mechanization. *Transactions of the Chinese Society for Agricultural Machinery*, Vol.49, No. 5, pp. 1-20.
[10] Liu F., Li D.P., Zhang T.et al., (2020). Analysis and calibration of quinoa grain parameters used in a discrete element method based on the repose angle of the particle heap. *INMATEH-Agricultural Engineering*, Vol.61, No. 2, pp.77-86.
[11] Ma X.J., Hou Z.F., Liu M., (2022). Calibration of simulation parameters of coated particles and analysis of experimental results. *INMATEH-Agricultural Engineering*, Vol.67, No. 2, pp.233-242.
[12] Nan W.G., Gu Y.Q., (2020). Stress analysis of blade Rheometry by DEM simulations. *Powder Technology*, No. 376, pp. 332-341.
[13] Qi L., Chen Y., Sadek M., (2019). Simulations of soil flow properties using the discrete element method (DEM). *Computers & Electronics in Agriculture*, No. 157, pp. 254-260.
[14] Roessler T., Katterfeld A., (2018). Scaling of the angle of repose test and its influence on the calibration of DEM parameters using upscaled particles. *Powder Technology*, No. 330, pp. 58-66.
[15] Rojek J., Lumelskyj D., Nosewicz S. et al., (2019). Numerical and experimental investigation of an elastoplastic contact model for spherical discrete elements. *Computational Particle Mechanics*, Vol.6, No. 3, pp. 383-392.
[16] Sun G.D., (2017). *Study of the device for seedling mud lifting and conveying on rice paddy field.* South China Agricultural University.
[17] Tamás K., Jóri I.J., Mouazen A.M., (2013). Modelling soil–sweep interaction with discrete element method. *Soil and Tillage Research*, No. 134, pp. 223-231.
[18] Wang L., Hu C., He X.W. et al., (2021). A general modelling approach for coated cotton-seeds based on the discrete element method. *INMATEH-Agricultural Engineering*, Vol.63, No. 1, pp.221-230.
[19] Wang W.P., Liu J.L., Zhang J.B. et al., (2014). Evaluation and correction of measurement using diffraction method for soil particle size distribution. *Transactions of the Chinese Society of Agricultural Engineering*, Vol.30, No. 22, pp. 163-169.
[20] Wang X.Z., Zhang Q.K., Huang Y.X. et al., (2022). An efficient method for determining DEM parameters of a loose cohesive soil modelled using Hysteretic Spring and Linear Cohesion contact models. *Biosystems Engineering*, No. 215, pp. 283-294.
[21] Xiang W., Wu M.L., Lü J.N. et al., (2019), Calibration of simulation physical parameters of clay loam based on soil accumulation test. *Transactions of the Chinese Society of Agricultural Engineering*, Vol.35, No. 12, pp. 116-123.
[22] Xu B., Zhang Y.Q., Cui Q.L.et al., (2021). Construction of a discrete element model of buckwheat seeds and calibration of parameters. *INMATEH-Agricultural Engineering*, Vol.64, No. 2, pp.175-184.
[23] Xu Y., Li H.Y., Huang W.B., (2003). Modeling and methodological strategy of discrete element method simulation for tillage soil dynamics. *Transactions of the Chinese Society of Agricultural Engineering*, Vol. 19, No. 2, pp. 34-38.
[24] Yang H.J., Wei F.Q., Hu K.H. et al., (2017). Effects of mud slurry on flow resistance of cohesionless coarse particles. *Powder Technology*, No. 310, pp. 1-7.

[25] Ye S.Q., (2021). Wet seedling raising technology in paddy field in southern Jiangxi. *Primary Agricultural Technology Extension*, Vol.9, No. 12, pp. 1-5.
[26] Zeng F.D., Li X.Y., Zhang Y.Z. et al., (2021). Using the discrete element method to analyze and calibrate a model for the interaction between a planting device and soil particles. *INMATEH-Agricultural Engineering*, Vol.63, No. 1, pp.413-424.
[27] Zeng Z.W., Ma X., Cao X.L. et al., (2021). Critical Review of Applications of Discrete Element Method in Agricultural Engineering. *Transactions of the Chinese Society for Agricultural Machinery*, Vol.52, No. 4, pp. 1-20.
[28] Zhang P., Zhang H., Li J.M.et al., (2022). Parametric calibration of cotton straw parameters in Xinjiang based on discrete elements. *INMATEH-Agricultural Engineering*, Vol.67, No. 2, pp.314-322.
[29] Zhang P.T., Sun X.J., Zhou X.J. et al., (2022). Experimental simulation and a Rapid reliable calibration method of rockfill microscopic parameters by considering flexible boundary. *Powder Technology*, No. 396, pp. 279-290.
[30] Zheng Z.Q., Zhao H.B., Liu P. et al., (2021). Maize straw cutting process modelling and parameter calibration based on discrete element method (DEM). *INMATEH-Agricultural Engineering*, Vol.63, No. 1, pp.461-468.
[31] Zhou J.C., Zhang L.B., Hu C. et al., (2022). Calibration of wet sand and gravel particles based on JKR contact model. *Powder Technology*, No. 397, pp. 117005.